Appl. Phys. A 61, 81–86 (1995)

Applied Physics A Materials Science & Processing

Mechanisms of melt droplets and solid-particle ejection from a target surface by pulsed laser action

A.B. Brailovsky, S.V. Gaponov, V.I. Luchin

Institute for Physics of Microstructures, Russian Academy of Sciences, 46 Ulianov Street, 603600 Nizhny Novgorod, Russia
(Fax: 78312/361972, E-mail: BRAIL@ipm.nnov.su)

Received: 19 March 1994/Accepted: 5 January 1995

Abstract. We suggest an explanation of the effect of melt droplets and solid particle ejection from a target surface under the impact of laser radiation with intensity 10^8–10^{10} W/cm^2. We consider the capillary wave instabilities on the evaporating surface of melt, which lead to growth of large-scale surface structures and ejection of macroparticles. The instability increments and characteristic droplet sizes are determined. Conditions are found for droplet-free evaporation in terms of the dynamic pressure of evaporated matter.

PACS: 79.20.DS

An important condition that allows application of laser-plasma technology is the absence of debris in ablation products, such as droplets or solid particles of target material. These can be formed through condensation of expanding gas or plasma during cooling [1], due to oversaturation in the region of plasma flux collision with an obstacle such as a substrate or another flux [2]. The presence of droplets and solid particles of the target material in the ablation flux can be a result a of their ejection directly from the target [3].

The condensation droplets typically occur in long-pulse and low-intensity regimes [4]. In the range of radiation parameters of interest (a pulse duration $\tau \simeq 30$ ns and intensity $q \simeq 10^8$–10^{10} W/cm^2) the condensation droplets are formed under a relatively slow expansion of the plasma into the background medium [5], or when the flux is disturbed by a substrate. Their typical radius is $r \simeq 10$–100 nm.

Along with small droplets, larger ones of sizes up to 1 μm were also observed during film deposition, as well as solid debris with a radius of about 10 μm. The amount and dimensions of macroparticles are determined by the material properties, radiation parameters and height of surface relief [3, 6].

The liquid splashing from the target surface is thought to be connected with the boiling of the melted layer and, for surface evaporation, to expulsion of melt by the impact of vapor pressure gradients. The gradients in the target plane may be related to laser beam inhomogeneity [7] or to a small-scale surface instability developing in the field of a polarized light wave [8]. However, one is unable to explain the formation of big droplets and debris in the framework of these models.

In this paper we suggest mechanisms of macroparticle ejection which are effective in the absence of definite polarization of the light wave and spatial modulation of the radiation intensity. They are related to the development of a surface melt instability in the field of plume plasma pressure and to growth of Large-scale Surface Structures (LSS) with a characteristic period of 20–30 μm [9, 10]. The droplets are believed to be formed due to breakaway of liquid at the peak of an aperiodically unstable capillary wave [11]. An approximate criterion for the ejection of droplets is proposed, which includes comparison of the surface energy of a forming droplet with the kinetic energy of the surface layer element whose velocity is equal to the velocity of instability growth, and the volume – to the volume of the droplet. Three types of instability leading to droplet formation and macroparticle ejection from the melt surface are considered.

The first mechanism is associated with the instability of the plane front of liquid evaporation [12]. We showed [9, 10] that such an instability leads to the formation of LSS due to a spatial modulation of the pressure in the near-surface plasma layer, followed by melt outflow from pits to humps and subsequent solidification. In materials for which the instability growth velocity is high enough for the above-mentioned criterion to be fulfilled, droplet ejection prevents the formation of LSS.

The second mechanism works if the condition for droplet ejection during one pulse is not met. In this case, droplets can be formed by multipulse relief formation as a result of the outflow of melted material from pits to humps. When flowing around the convex areas, the liquid is in the field of the centrifugal force, which may induce

a Rayleigh–Taylor-type instability at the liquid–vapor interface.

The third mechanism by which the droplets enter the ablation flux acts at the nonlinear stage of the relief formation when the humps transform into vertical columns. The vapor velocity is much higher than the velocity of liquid layer, and the Kelvin–Helmholtz instability develops on the column surface. The instability development over one pulse results, just like in the previous cases, in the ejection of droplets. By a multiple-pulse irradiation of the target, the formation and ejection of spherical macroparticles with a radius $r \simeq 10\ \mu$m can be achieved.

Besides the three droplet-ejection mechanisms which are analyzed in this paper, one can imagine a number of other instabilities producing the same effect. For example, when matter is evaporated from small areas and the spread of vapor and melt along the target surface is an essential factor, there is a possibility for development of a shear flow instability (spread of vapor) [11, 13] and a Rayleigh–Taylor instability [14] (a boundary acceleration due to the lateral spread of the melt). The specific droplet-ejection mechanism is determined by instability increments which depend upon evaporation conditions.

1 Capillary-wave instability in the field of plume pressure

The melt-surface instability under laser evaporation of absorbing targets has been considered in [7–12, 15, 16]. The gas-dynamic disturbances in the flow of evaporated matter have sufficient effect on the behavior of the interphase boundary, when subsonic vapor outflow occurs [12]. The condition $M < 1$ (M is the Mach number on the target surface) is connected with the absorption of radiation by the laser plume and its heating in our evaporation regime. In [9, 10] it is shown that space modulation of pressure in the plasma surface layer arises due to local focusing and defocusing of the flux of evaporated substance which is directed along the normal to the target surface. The pressure near the concave region of surface is higher than that above the convex part of the relief. Due to pressure gradients the molten surface layer flows from pits to relief humps and the local curvature of the surface increases, the depth of pressure modulation grows, etc. The dispersion equation, describing this capillary-wave instability has the form

$$\omega^2 = \frac{1}{\rho_1}(-\rho_0 v_0^2 \beta k^2 + \sigma k^3), \tag{1}$$

where ρ_0 and v_0 are the density and mass velocity, $\beta = (1 - M^2)^{-1/2}$, and ρ_1 and σ are the density and the surface tension coefficient of liquid. For a sufficiently rapid growth of the capillary-wave amplitude, the liquid is likely to splash along the normal to the target (Fig. 1). To estimate the size of droplets formed in this process, we take [11] $r = \lambda_m/4$, where the wavelength which corresponds to the maximum instability increment is

$$\lambda_m = \frac{3\pi\sigma}{\rho_0 v_0^2 \beta}. \tag{2}$$

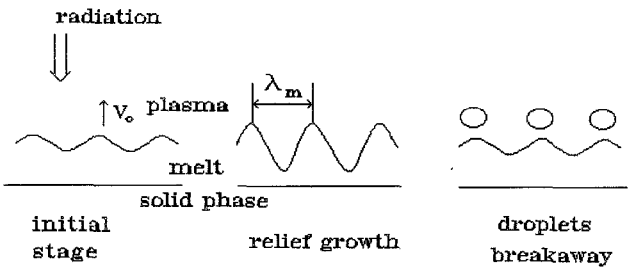

Fig. 1. Scheme to explain the melt-droplet formation and breakaway

The condition for breakaway of droplets with the volume $V = (4/3)\pi r^3$ is found by comparison of the kinetic energy $0.5\rho_1(\partial\zeta/\partial t)^2 V$ of the given liquid volume with the surface energy of the droplet $4\pi r^2\sigma$; here ζ is a sinusoidal perturbation of the melt surface

$$\rho_1\left(\frac{\partial\zeta}{\partial t}\right)^2 \geqslant \frac{6\sigma}{r}. \tag{3}$$

Substitution of $\partial\zeta/\partial t = \Gamma_m\zeta$, where $\Gamma_m = 2\rho_0^{3/2} v_0^3 \beta^{3/2}/(3\sqrt{3\rho_1\sigma})$ is the maximum instability increment, yields

$$\zeta \geq 0.44\ \lambda_m. \tag{4}$$

Thus, for the droplets to break away it is required that the capillary-wave amplitude reaches this value during the time of intensive evaporation, i.e., on the condition that

$$\zeta_0 \exp(\Gamma_m \tau) \geq 0.44\ \lambda_m, \tag{5}$$

where ζ_0 is the amplitude of the incipient melt-surface perturbation at the wavelength λ_m. The droplet-formation condition is realized by irradiation of materials with a low evaporation temperature and high values of instability increment, which primarily depends on $\rho_0 V_0^2$. Let us give estimates of the parameters in formula (5) for the case of bismuth. To determine ρ_0, v_0 and M we utilize the solution of the problem for laser evaporation into a background medium [17]. Necessary data on the intensity of radiation absorbed by the target and the density of the evaporated particle flux, j, have been obtained by us experimentally (unpublished). For the incident radiation intensity $q_0 = 10^9$ W/cm^2; $q_s = 1.5 \times 10^7$ W/cm^2 comes through the plasma and is absorbed by the target. The flux j is equal to 3×10^{-25} cm^{-2} s^{-1}. These parameters correspond to the following characteristics of the evaporated matter flux at the target surface: $\rho_0 = 0.5$ g/cm^3, $v_0 = 3 \times 10^4$ cm/s, and $M = 0.6$. From (2) and (3) we obtain $\lambda_m = 10^{-5}$ cm and $\Gamma_m = 2 \times 10^9$ s^{-1}. With these values, condition (5) can be achieved for 3 ns of intensive evaporation on an atomically smooth surface of bismuth.

Analyzing the dispersion equation (1) with the help of relation (5), one can pick out the part in the wave number region corresponding to the melt surface instability, for which the breakaway condition is fulfilled over the duration of one pulse, and, in this way, estimate the size distribution of droplets.

2 Rayleigh–Taylor instability of the melt surface on convex areas of the relief

In case where the condition of droplet ejection (5) is not fulfilled during one-pulse evaporation of matter, the droplets may be formed by multipulse irradiation of the target. When deriving the dispersion equation (1), we did not take into account the role played by the dynamic pressure of liquid along the surface, assuming that $1/2\rho_1 U^2 \ll \rho_0 v_0^2 \beta k\zeta$ and $\sigma(\partial^2\zeta/\partial x^2 + \partial^2\zeta/\partial y^2)$, where U is the liquid velocity along the target surface. Let us now estimate how the process of relief formation changes when the liquid layer flows around convex areas. The centrifugal force can bring about the Rayleigh–Taylor instability at the liquid-vapor interface (Fig. 2). The characteristic acceleration in this case is $g = U^2/R$, where R is the radius of the liquid–solid boundary curvature. If R is comparable with the relief wavelength, its value may be estimated as $R \simeq \lambda_n/4$; if $R \gg \lambda_n$, then $1/R = k_n^2\zeta_n$, where ζ_n is the relief amplitude formed at the moment of the arrival of this pulse, and k_n and λ_n are the wavenumber and wavelength of LSS.

The dispersion equation for the capillary waves in the field of the centrifugal force can be written as

$$\omega^2 = -\alpha_0 \frac{U^2}{R} k + \frac{\sigma}{\rho_1} k^3, \tag{6}$$

where [18] $\alpha_0 = (\rho_1 - \rho_0)/(\rho_0 + \rho_1) \simeq 1$. From this equation we find the optimal wavelength and wave number

$$\Lambda_m = \frac{2\pi\sqrt{3\sigma R}}{U\rho_1^{1/2}}, \quad k_m = U\left(\frac{\rho_1}{3R\sigma}\right)^{1/2}, \tag{7}$$

corresponding to the maximum instability increment $\gamma_m = 0.62U^{1/2}\rho_1^{1/2}/(R^{3/4}\sigma^{1/4})$.

To estimate the melt flow velocity along the target surface and the time for which this velocity remains high, let us use the following model. The relief humps are assumed to be cylinders with a height $2\zeta_n$ and radius $\lambda_n/4$. During the evaporation time, the hump height rises, due to the flow of a melt portion with a volume $\Delta V_+ = \pi/4b\tau^2\lambda_n H_1$ along the melt layer with the thickness H_1 on the side of the cylinder over its entire perimeter. Here b is the liquid acceleration along the target surface estimated [9] as $b = (1/\rho_1)(\rho_0 v_0^2 \beta k_n^2\zeta_n - \sigma k_n^3\zeta_n)$ for $\zeta_n \ll \lambda_n$. By the end of the pulse the velocity amounts to

$$U_0 = k_n^2\zeta_n\tau/\rho_1(\rho_0^2 v_0\beta - \sigma k_n). \tag{8}$$

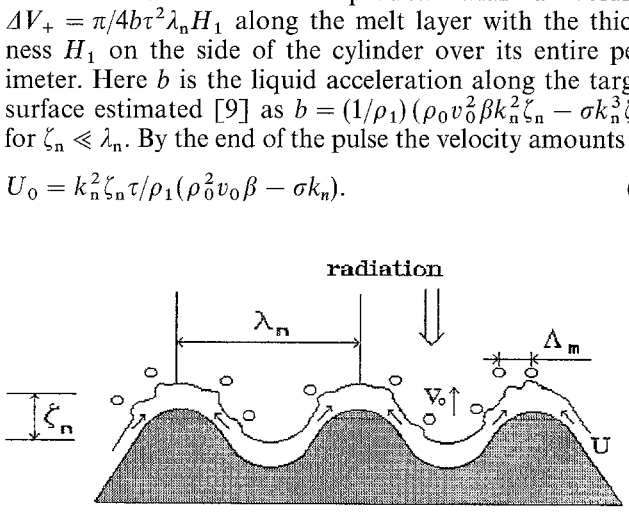

Fig. 2. Droplet formation due to Rayleigh–Taylor instability at the convex areas of relief

After the end of the pulse, it falls off as $U = U_0 - ct$, where $c = \sigma k_n^3/\rho_1\zeta_n$ and the time t is counted from the moment at which evaporation stops. By the moment τ_1 when the melt solidifies, the cylinder volume will change by the value $\Delta V = U_0\tau_1 - 1/2c\tau_1^2$. Thus, the increase of the cylinder height under one pulse irradiation is estimated as

$$\Delta\zeta_n = \frac{2\zeta_n H_1 k_n^3}{\pi\rho_1}[\rho_0 v_0^2\beta\tau(\tau + 2\tau_1) - \sigma k_n(\tau + \tau_1)^2]. \tag{9}$$

The duration of evaporation is assumed to be equivalent to the pulse duration. We use the condition $d(\Delta\zeta_n)/dk_n = 0$ to find the wavenumber of the surface structure

$$k_n = \frac{3\rho_0 v_0^2\beta\tau(\tau + 2\tau_1)}{4\sigma(\tau + \tau_1)^2}. \tag{10}$$

To find out the time dependence of the liquid layer thickness $H_1(t)$ and the time of melt solidification τ_1, one needs to solve a problem of surface cooling taking into account the phase boundary motion. Here we restrict ourselves to a rough estimates of τ_1, using the relation $T_b\rho_1 c_1\sqrt{a\tau} \simeq T_m\rho_1 c_1\sqrt{a\tau_1}$ which yields $\tau_1 \simeq \tau(T_b/T_m)^2$. Here T_b is the melt boiling temperature, T_m is the melting temperature, c_1 is the heat capacity and a is the thermal diffusity. The melting temperature for many materials is approximately 0.3 of the boiling temperature [19], and $\tau_1 \simeq 10\tau$. Noting that $\tau \ll \tau_1$ we write down the following expression for velocity U_0:

$$U_0 \simeq \frac{2(\rho_0 v_0^2\beta)^3\tau^3}{\sigma^2\tau_1^2}\zeta_n. \tag{11}$$

We search for the condition of droplet breakaway in the form (3), as earlier. For the case of the Rayleigh–Taylor instability on convex areas of the relief, we obtain the criterion

$$\zeta_0 \exp(\gamma_m\tau_0) \geq 0.22\,\Lambda_m, \tag{12}$$

where γ_m and Λ_m are determined by the relation (7), and τ_0 is the time during which the flow velocity remains high enough. For estimates we take τ_0 equal to $\tau + U_0/c$ — the time interval up to the moment when the melt stops flowing on the humps of relief. Taking account of (9) and (11), we obtain $\tau_0 \simeq 0.7\tau_1$. By specifying the initial amplitude of the surface profile perturbation at $\zeta_0 = 10^{-8}$–10^{-6} cm, we find from (12) the condition for droplet breakaway $\gamma_m\tau_0 \geq 5$–9 (for brass). Taking $\ln(\Lambda_m/\zeta_0) = 5$ (due to the logarithmic dependence on Λ_m and ζ_0, the droplet breakaway criterion is determined for any material by the value $\gamma_m\tau_0$), we have

$$\frac{(\rho_0 v_0^2)^6\beta^6\zeta_n^{9/4}\tau^{3/2}\tau_1}{\rho_1^{5/4}\sigma^{19/4}} > 240. \tag{13}$$

Let us estimate for a brass target the amplitude of relief that, under flow of melt, causes droplet ejection. When $\rho_0 = 0.02$ g/cm^3, $v_0 = 2\times10^4$ cm/s, $\rho_1 = 8.5$ g/cm^3, $\sigma = 900$ erg/cm^2, $\tau = 3\times10^{-8}$ s, $\beta \simeq 1$, we have the condition $\zeta_n \geq 10$ μm.

To utilize the droplet-ejection criterion (12), it is necessary to meet some other conditions. Since the

Rayleigh–Taylor instability can develop only on convex parts, when the melt flows from the average level of relief to its peak, the droplet can be formed only if more than a half-wave $\Lambda_m/2$ fits into a part of length $\lambda_n/4$, i.e., $\Lambda_m < \lambda_n/2$. Using (10) we write the inequality in the form:

$$\zeta_n > \frac{\sqrt[3]{3}\sigma^{5/3}\rho_1^{1/3}\tau_1^{4/3}}{(\rho_0 v_0^2)^2\beta^2\tau^2}. \tag{14}$$

This condition proves to be more rigid than (13) if $\delta = \rho_0 v_0^2 \beta \sigma^{-2/3}\rho_1^{-1/3}\tau^2 > 2.1$. With a further increase of the parameter $\rho_0 v_0^2\beta$ (low vaporization heat materials), starting at $\delta > 13$ the droplet-ejection condition (5) becomes effective due to instability development on a plane surface. The latter inequality is equal to the condition $\Gamma_m\tau > 5$. In this case, droplet ejection starts with the first pulses, and there is no surface relief formation.

By writing the dispersion equation for capillary waves in the field of centrifugal force as (6), we implied that the melt flow velocity along the surface is constant. Nevertheless, the stationary velocity cannot be achieved. Velocity variation can be neglected when deriving the dispersion equation, if $dU/dt \ll U\gamma_m$. This relation is not fulfilled during the liquid acceleration when $t < \tau$. But the longest phase of the Rayleigh–Taylor instability development from $t = \tau$ to $t = \tau_1$ takes place when the melt flow slows down at $\partial U/\partial t \simeq \sigma k_n^3/\rho_1\zeta_n$. Comparison of this expression with $U\gamma_m$ yields the condition for a quasistationary state of flow $\gamma_m\tau_1 \gg 3$ which is roughly met in the case of droplet ejection ($\gamma_m\tau_1 > 8$).

3 Kelvin–Helmholtz instability at a vertical boundary of relief and ablation flux

Let us now consider one more type of instability that can bring droplets into the ablated material flux. The nonlinear phase of surface relief development is characterized by the growth of vertical columns. The ablation flux flows along these throughout the pulse at a velocity that is much higher than that of the melt streaming up the column wall. The melt–vapor boundary is the surface of shear flow (Fig. 3a). The dispersion equation for capillary waves on a liquid surface with $\rho \ll \rho_1$ has the form [18] similar to (1):

$$\omega^2 = \frac{1}{\rho_1}(-\rho v^2 k^2 + \sigma k^3). \tag{15}$$

The ablated material flux velocity v is connected with the mass velocity v_0 on the target surface via the continuity equation $\rho_0 v_0 = \rho v$. Therefore, the instability increment γ_T exceeds the increment Γ_m responsible for relief growth, because ablation plasma is accelerated by laser heating, i.e.,

$$\gamma_T = \frac{2(\rho v^2)^{3/2}}{3\sqrt{3}\rho_1^{3/2}\sigma} = \Gamma_m(v/v_0)^{3/2}.$$

The condition for droplet formation by this mechanism is expressed by the inequalities $\gamma_T\tau > 5$ and $\Gamma_m\tau < 5$, since, besides droplet breakaway from columns walls, it is required that no intensive droplet ejection takes place during the phase when the relief is being formed. From this we find the parameter range in which the conditions hold for droplets breakaway from the columns walls:

$$13 v_0/v\beta < \rho_0 v_0^2 \beta(\sigma\rho_1)^{-2/3}\tau^{2/3} < 13.$$

Plasma expansion during a pulse has a complicated dynamics and numerical calculations are required to find the flow velocity. In order to estimate v, we utilize the velocity dependence on distance from the target x, determined by the self-consistent evaporation model [20]: $v = v_0(1 + 17/4\, x/x_{fr})$, where x_{fr} is the plasma-front coordinate. Let us take $x = H_c$ (column height) and $x_{fr} = v_{fr}\tau$ (here v_{fr} is the front velocity). Then, the condition for droplet breakaway from the column has the form:

$$\rho_0 v_0^2 \sigma^{-2/3}\rho_1^{-1/3}\tau^{2/3}(1 + 17/21\, H_c/v_0\tau) > 13. \tag{16}$$

The relations obtained are valid under certain conditions. The time of instability development t is limited by the time of perturbation drift to a distance equal to the column height. In the dispersion equation (15), we neglected the real part $kv\rho/(\rho + \rho_1)$. Taking into account that the perturbation drift velocity is

$$v\rho/(\rho + \rho_1) \simeq \rho_0 v_0/\rho_1,$$

we have $t < \rho_1 H_0/(\rho_0 v_0) = H_0/v_{ev} \gg \tau$. Here v_{ev} is the evaporation velocity. After some time, perturbation drift due to melt flow may become an important factor. Estimating this drift over time t as $\Delta x \simeq (\rho_0 v_0^2)^2/(\rho_1\sigma)(\tau/\tau_1)\tau^2$, from the condition $\Delta x < H_c$, we obtain the restriction on the time of instability development (for brass when $H_c \simeq 10^{-3}$cm, $t < 4 \times 10^{-3}$ s). It is also necessary to take into account natural factors limiting the instability wavelength: $\lambda_T/2 < H_c$ and $\lambda_T \ll 2\pi R_c$, where $R_c = \lambda_n/4$, or $H_1 > 3\pi\sigma/(2\rho_1 v^2)$ and $v/v_0 \gg 3\tau/\tau_1 \simeq 0.3$, here R_c is the column radius. Estimates show that the above restrictions are not rigid, and the conditions for droplet ejection from the column walls reduce to (16).

The mechanisms under study thus allow the formation of droplets with an average radius $r \simeq 10^{-6}$–10^{-4} cm. Along with these, larger particles with $r \simeq 10^{-3}$ cm were observed on a substrate placed in the path of the

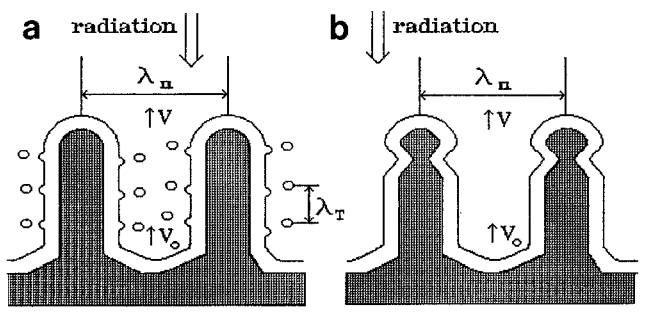

Fig. 3a, b. Scheme of melt-droplet (**a**) and solid-particle (**b**) formation and breakaway due to Kelvin–Helmholtz instability at the vertical boundary of relief and ablation flux

expanding plasma. They are also likely to be due to shear flow instability, but large-size particles are formed by multiple rather, than single pulse irradiation of a target with a well-developed relief, containing vertical columns. For a waist to exist on a column with radius $R_c = \lambda_n/4$ at a distance from the peak equal to $2R_c$ (see Fig. 3b), it is required that the instability wavelength be $\Lambda_T = 2R_c = \lambda_n/2$. Still assuming the instability to develop over the time $\simeq \tau$, trying to find a spatial scale, we need to take into account the spread of column surface perturbation for the time of melt cooling, τ_1. By analogy with (10), we get

$$\Lambda_T = 4\pi\sigma\tau_1/(3\rho v^2\tau). \tag{17}$$

Then, using the condition $\Lambda_T = \lambda_n/2$ and $\rho_0 v_0 = \rho v$, we have $v = 2v_0$. Such a relation between the plasma velocity near the waist and the initial velocity of vapor seems to be quite realistic (it can be verified only by numerical calculations of the expansion dynamics).

When a column waist becomes thin enough, the ablated material flux tears off a ball and carries it away. It is affected by the frictional force of the flowing-round stream, by the force related to the flux velocity $F = \rho v^2 \pi R_c^2$, and by the force caused by the pressure gradient in a flux which may be estimated as $\nabla P \simeq \rho v/\tau = \rho_0 v_0/\tau = \rho_1 h^2/\tau$, where h is the depth of a crater produced by evaporation. The estimates for brass show that the major contribution to the ball acceleration is made by the forces related to the velocity and to the pressure gradient ($\nabla P = 4 \times 10^{10}$ dyn/cm^3), and the velocity of the ball becomes $v_s \simeq 300$ cm/s for the time τ. To break a melt waist with a radius r_w it is enough to use the energy $\Delta E = 2\pi r_w^2 \sigma$. From the relation $1/2\ m_s v_s^2 > \Delta E$ (here m_s is the mass of the ball), we find the waist radius when the ball breaks away: $r_w < 2 \times 10^{-4}$ cm. This estimate is in good agreement with the experimental data [9, 10] and the estimate for a melt layer thickness. The pulse-by-pulse dynamics of solid-ball formation and breakaway on the column peaks is presented in Fig. 4. One also can observe the smaller spherical particles in this figure. We believe that these particles return to the target with the backward plasma flux. Apparently that is the way droplets arrive at the target during the initial phase of relief formation (Fig. 5).

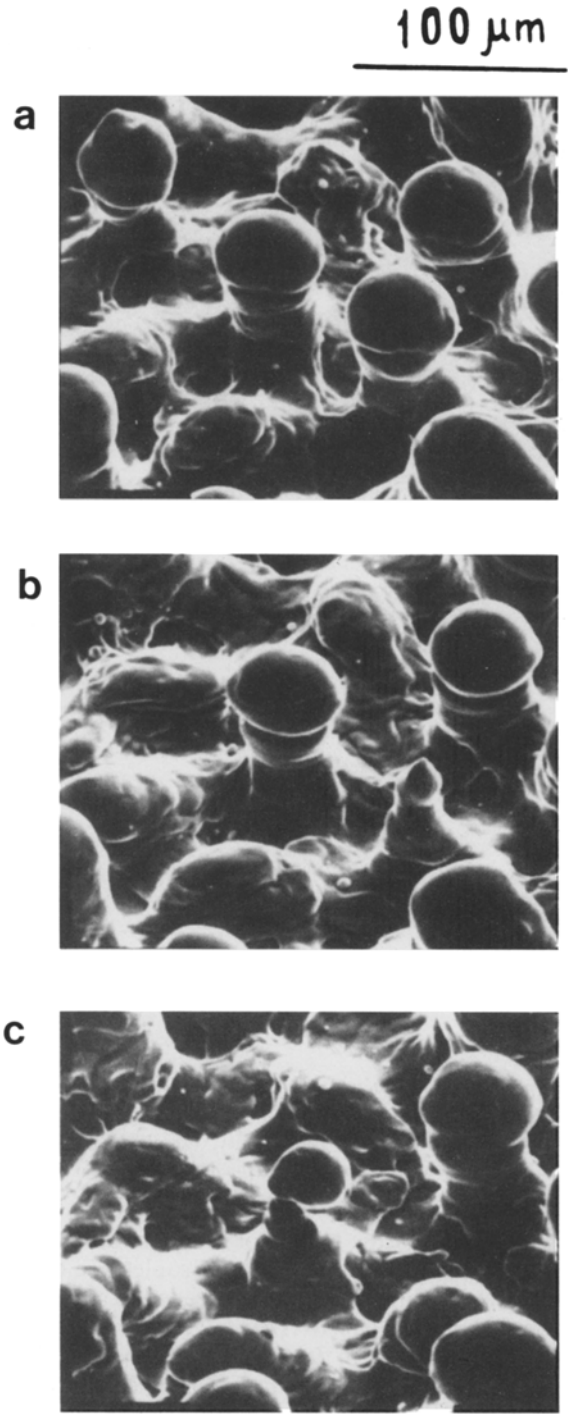

Fig. 4a–c. A brass target photographed after N pulses irradiation in vacuum (**a**) $N = 35$; (**b**) $N = 38$; (**c**) $N = 43$; $q = 10^9$ W/cm^2, $\tau = 30$ns, laser wavelength is 1.06μm

4 The conditions for ejection of macroparticles and their characteristic sizes

For droplets to eject by any of the above three mechanisms requires a capillary instability caused by the ablation plasma focusing above the pits and defocusing above the humps of relief. The present authors showed [9, 10] that this can be achieved by meeting the following conditions:

$$\kappa_0 < \frac{n_0 m^2 v_0^4 \beta^2}{4\Omega\sigma}, \tag{18}$$

where κ_0 is the plasma absorption coefficient near the target surface, Ω is the evaporation heat per particle, n_0 is the plasma concentration and m is the mass of an evaporated particle. As the laser intensity increases, the temperature and κ_0 grow faster than the evaporation velocity and the parameter $n_0 v_0^4$, the latter being limited by an increasing backward flux of particles. Thus, besides the droplet-ejection criteria (5), (12), and (16) which are related, primarily, to the properties of evaporated matter, there is also condition (18) which depends mainly on laser radiation intensity. The analysis of these relations could

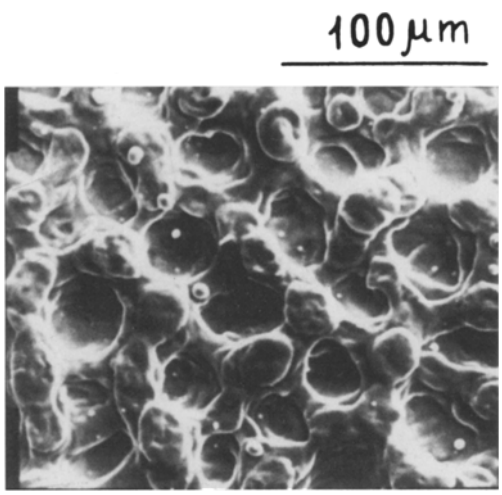

Fig. 5. View of surface after 6 pulses of irradiation; $q = 10^9$ W/cm^2

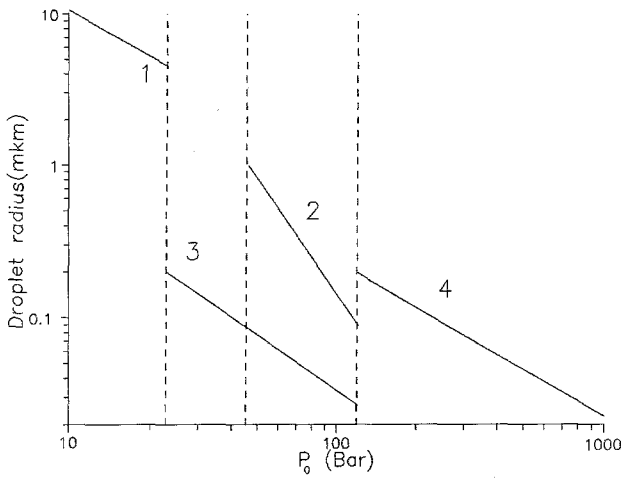

Fig. 6. The dependence of characteristic droplet and solid-particle radius on the parameter p_0 for different ejection mechanisms. *1*, Solid particles; *2*, Rayleigh–Taylor instability; *3*, Kelvin–Helmholtz instability; *4*, focusing and defocusing of plasma flux

allow determination of the ranges of the main laser radiation parameters which correspond to droplet-free evaporation. But numerical calculation are needed to solve this problem. In this paper we restrict ourselves to the analysis of the above conditions in terms of the most strongly varying parameter $p_0 = \rho_0 v_0^2$ (or $\rho_1 v_{ev} v_0$), which is part of the condition for LSS formation and droplet ejection and is responsible for droplets entering the ablation flux. The values of σ and ρ_1 used for estimations are averaged over a variety of materials.

The dependencies of the droplet and solid-particle radius for different instabilities on the parameter p_0 are given in Fig. 6. The droplet sizes are obtained from estimations of characteristic wavelengths of corresponding instabilities [formulas (2), (7), (11) and (17)]. Vertical dashed lines define the boundaries of areas which correspond to instability development [formulas (5), (12) and (16)]. We assume that liquid ejection during one pulse prevents the relief formation; this is why curves 2 and 3 are restricted by a dashed right line. The curve 1 is restricted on the right since droplet ejection due to a Kelvin–Helmholtz instability prevents ball formation. The droplet size limitation $r \leq 10^{-6}$ cm is connected with the free path of atoms 1 in vapor. The hydrodynamic flow begins at a distance $x = (2\text{–}3)1$ from the target surface [17]. We assume that the hydrodynamic description, used in the analysis of the interphase boundary stability, is valid if $\lambda_n > 31$. It follows from this condition that the droplet size is limited from below by a value $\simeq 10^{-6}$ cm.

5 Conclusion

The paper gives an explanation for the ejection of droplets and solid particles from a target surface, as observed in studies of laser deposition. The proposed models have allowed us to find the characteristic sizes of droplets and the conditions for droplet formation as a function of the parameters of ablation flux. The authors are the first to report a mechanism of solid particles entering into an ablation flux, which is related to the development of large-scale relief on a target surface. The LSS growth is shown to be one of the conditions for droplet ejection. Based on the well-known dependencies of structure growth rate on wavelength [6] and intensity [9, 10] of laser radiation, one can try to optimize the irradiation conditions to find the droplet-free regimes of evaporation.

Acknowledgements. The authors are grateful to I.A. Dorofeev and V.E. Semenov for fruitful discussions and to V.A. Ermakov for support in the electron microscopy work.

References

1. J. Saito, K. Mihama, T. Noda: Jpn. J. Appl. Phys. **22**, L715 (1983)
2. S.V. Gaponov, A.A. Gudkov, A.A. Fraerman: J. Tech. Phys. **52**, 1843 (1982)
3. J.F. Ready: Appl. Phys. Lett. **3**, 11 (1963)
4. A. Richter: Thin Solid Films **188**, 275, (1990)
5. H.U. Hebermeier, G. Beddies, B. Leibold, G. Lu, G. Wagner: Physica C **180**, 17 (1991)
6. W. Kautek, B. Roas, L. Schultz: Thin Solid Films **191**, 317 (1990)
7. V.N. Anisimov, B.V. Arutyunyan, V. Yu. Baranov, L.A. Bolshov, O.N. Derkach: Appl. Opt. **23**, 18 (1984)
8. R.B. Arutyunyan, L.A. Bolshov, M.A. Dunayevski, V.P. Reshetin: Dok. Akad Nauk SSSR **316**, 347 (1991)
9. A.B. Brailovsky, A.B. Ezersky, I.A. Dorofeev, V.A. Ermakov, V.I. Luchin, V.E. Semenov: J. Tech. Phys. **61**, 129 (1991)
10. A.B. Brailovsky, S.V. Gaponov, I.A. Dorofeev, V.I. Luchin, V.E. Semenov: SPIE Proc. **1440**, 84 (1990)
11. R.L. Johnson, J.D. O'Keefe: AIAA J. **8**, 1106 (1974)
12. E.B. Levchenko, A.L. Chernyakov: J. Appl. Mech. Tech. Phys. **2**, 144 (1982)
13. V.N. Golubev, I.A. Dorofeev, M.N. Libenson, V.I. Luchin: Pishma J. Tech. Phys. **24**, 67 (1991)
14. Ju. A. Chivel: Kvant. Electron. **10**, 1218 (1991)
15. H.J. Palmer: J. Fluid Mech. **75**, 487 (1976)
16. A.I. Korotchenko, A.A. Samokhin, A.P. Gus'kov: Appl. Phys. A **27**, 121 (1992)
17. C.J. Knight: AIAA J. **5**, 519 (1979)
18. L.D. Landau, E.M. Livshitz: *Gidrodinamica* (*Hydrodynamics*) (Nauka, Moscow 1986) (in Russian)
19. A.P. Babichev, N.A. Babushkina: *Fizicheskie velichiny* (*Physical values*), ed. by I.S. Grigoriev, E.Z. Meilikhov (Energoatomizdat, Moscow 1991) (in Russian)
20. O.N. Krokhin: In *Laser Handbook*, ed. by F.T. Arecchi, E.O. Schulz-Dubois, Vol. 2 (North-Holland, Amsterdam 1972) p. 1371